Evaluation of the deformity of congenital proximal radioulnar synostosis by using a digital technique

Chen Yang
Beijing Jishuitan Hospital
Lu Liu
Beijing Jishuitan Hospital
Qi-Pei Wei
Beijing Jishuitan Hospital
Fan Bai
Beijing Jishuitan Hospital
Shan-lin Chen (drcsl@qq.com)
Beijing Jishuitan Hospital

Research Article

Keywords: Deformity, Digital orthopedic, Forearm, Radioulnar synostosis

Posted Date: October 6th, 2022

DOI: https://doi.org/10.21203/rs.3.rs-2075445/v1

Abstract

Purpose: To find out the influence factors of the “forearm rotation angle” (FR) which related to the severity of CRUS.

Methods: We established 48 digital three-dimensional forearm bones models of 48 patients with congenital radioulnar synostosis (CRUS) classified as Cleary and Omer type 3. In total, 10 independent deformities involved in the CRUS complex deformity were measured. Pearson correlation analysis for each deformity was performed and multivariate linear regression analysis was also performed with FR as the dependent variable and the other deformities as the influential factors.

Results: The “dorsal angle of radius” (DAR) had the strongest correlation with the FR (0.601, $P<0.01$), the internal rotation angle of the radius (IRAR) has a moderate correlation with FR (0.552, $P<0.01$). A forearm deformity equation was established: FR=35.896+0.271 DAR+0.989 IRAR.

Conclusion: The results of this study and the forearm deformity equation may be significant in guiding clinical practice.

Level of Evidence: Level 4 Evidence.

Introduction

Congenital radioulnar synostosis (CRUS) is a rare congenital deformity of the upper extremity, which usually presents as a pronation deformity of the forearm. It can be bilateral or unilateral. In severe cases, the patient cannot complete movements, such as carrying a bowl, and writing, which affect the patient's daily life, work, social activities, and hobbies.[1]

Cleary et al.[2] classified the disease into four types according to the radial head dislocation and the osseous synostosis condition at the proximal radioulnar joint (PRUJ) on plain radiographs. The most common type is type 3,[3, 4] which is characterized by the posterior dislocation of the radial head. Kanaya et al. treated the patients by reconstructing the shape of PRUJ and proximal radius, and overcame the problem of the high rate of postoperative re-ankylosis with the traditional method.[5–10] However, the outcome is not so good unanimously. As the bone structure of CRUS forearm is not so simple as we imagine (Fig. 1),[11–13] it is hard to correct every abnormal structure by performing this procedure. And the post-operative bony deformities might be important influential factors.

Therefore, it is very important to determine the bony malformation relationship of the CRUS forearm. However, the mechanisms on how the independent deformities influence the forearm pronation deformity and how they relate to each other have not been determined. Thus, we aimed to describe the deformities of CRUS more reliably by using digital 3-Demensional reconstruction technology, and to investigate the degree of influence of each individual deformity perimeter on the forearm pronation deformity and the correlation among the individual deformity perimeters, so as to provide a theoretical basis for improving the surgical treatment strategy.

Methods

This case series study obtained approval from the ethical review board of our institution, and all of the included patients provided informed consent. The inclusion criteria were as follows: patients who were treated at our institution from June 2016 to January 2010 and were classified as having type 3 deformities according to Cleary and Omer classification. Patients who were unwilling to undergo or unable to complete computed tomography (CT) examinations were excluded from this study.

Altogether 48 forearms of 48 CRUS patients (36 males and 12 females; age range: 1 to 28 years old) were included in the analysis. There were 15 and 33 patients with bilateral and unilateral involvement, respectively; of these, 22 and 11 patients had a deformity on the left and right sides, respectively. CRUS patients with a type 3 deformity on one side and another type on the other side were considered as having unilateral involvement.

Preoperative bilateral forearm CT examination was performed. During the examination, the patient was placed in the prone position, with both forearms raised, palms down, and elbows slightly flexed, and the forearms were scanned simultaneously. For bilateral cases, one side was randomly selected to be included in the study. Among the 15 bilateral cases, 8 right and 7 left forearms were included in the study. Digital model reconstruction software was used to conduct digital 3-D modeling using the DICOM files of forearm CT. The independent osseous deformities of CRUS were as follows[11−13]: 1) the radial diaphysis is in an arch shape, and its deformity is characterized by internal rotation, radial, and dorsal angulations; 2) the ulnar diaphysis deformity is characterized by internal rotation, ulnar, and palmar angulations; 3) osseous fusion of the PRUJ; 4) posterior dislocation of the radial head with a dysplastic and abnormal shape; 5) abnormal alignment of the humeroradial joint; and 6) dorsal dislocation of the ulnar head at the distal radioulnar joint (DRUJ).

The ulna and radius were separated according to the physiological traces at the proximal osseous synostosis part of CRUS, and the relevant data of the independent deformities were measured.

Forearm rotation angulation deformity

The angle between the axis of the humerus and the projection of the connecting line of the radial styloid process and the middle point of the ulnar head on the transverse plane was used as the forearm rotation angle (FR) (Fig. 2).

Radial deformities

In unilateral cases, the digital 3-D model of the bilateral radius was established, the model of the healthy side was reversed on the sagittal plane, and its distal articular surface and that of the affected side were superimposed using the interactive closest-point algorithm. In the bilateral cases, the model of the ipsilateral healthy radius from people of similar age was established and rescaled, and its distal articular surface was superimposed with the affected radius using the interactive closest-point algorithm. Then, the internal rotation, radial, and dorsal angulation deformities were measured. Given that the deformities were multi-plane, the measurement methods were standardized as follows: 1) the internal rotation angle of radius (IRAR): given that the landmarks at the proximal ulnar part of the radius in CRUS patients disappeared due to the osseous fusion, IRAR was measured on the transverse plane of the healthy radius, and the angle between the perpendicular line of the projection of the cutting edge at the proximal part of the affected radius and the connecting line of the incisura ulnaris and the center of the radial head of the healthy radius was used as the IRAR; 2) radial angle of the radius (RAR): given that the distal articular surfaces were superimposed, the projection of the angle between the proximal axis of the affected radius and the healthy radius on the coronal plane of the healthy radius was used as the RAR; and 3) dorsal angle of the radius (DAR): given that the distal articular surfaces were superimposed, the projection of the angle between the proximal axis of the affected radius and the healthy radius on the sagittal plane of the healthy radius was used as the DAR (Fig. 3).

Ulnar deformities

Similar to the measurement methods of the radial deformities, the model of the healthy side of the patient or the modified model of the ulna of the healthy person was superimposed at the humeroulnar articular surface and olecranon using the interactive closest-point algorithm. Given that the proximal parts were superimposed, the internal rotation, ulnar, and palmar angulation deformities of the ulna were measured using the following standardized methods: 1) internal rotation angle of the ulna (IRAU): the projection of the angle between the connecting line between the center of the ulnar head and ulnar styloid process of the affected ulna and the healthy ulna on the transverse plane of the healthy ulna was used as the IRAU; 2) ulnar angle of the ulna (UAU): the projection of the angle between the axis of the affected ulna and the healthy ulna on the coronal plane of the healthy ulna was used as the UAU; and 3) palmar angle of the ulna (PAU): the projection of the angle between the axis of the affected ulna and the healthy ulna on the sagittal plane of the healthy ulna was used as the PAU (Fig. 4).

Relative length of osseous synostosis (RLOS)

The RLOS was measured as the ratio of the longest diameter of the fusion site of the affected ulna to the distance between the center of the ulnar head and the midpoint of the olecranon tip (Fig. 5).

Proximal metaphysis of radius

Given that the cartilage of the radial head cannot be contoured clearly in the CT images, the relative transverse area of the proximal radial metaphysis (RAPAM) was chosen as the approximate indicator of the development of the radial head. Moreover, the RAPAM was measured as the ratio of the transverse area of the proximal metaphysis of the affected radius to the transverse area of the proximal metaphysis of the healthy radius (Fig. 6).

The relative distance of ulnar head dislocation (RDUD)

Ulnar head dislocation can be classified as palmar and dorsal dislocations, and was observed and classified. The RDUD was measured as the ratio of the projection of the vertical distance between the palmar margin of the ulnar head and the extension line of the radial palmar margin to the projection of the length of the sigmoid notch on the transverse plane (Fig. 7).

Statistical analysis

The distribution of each deformity perimeter and the Pearson correlation among the perimeters of normal distribution was analyzed. The scatterplot between the FR and the other deformity perimeters was mapped to eliminate the index that was not linearly correlated with the FR. The analysis of variance (ANOVA) of each deformity index was performed to eliminate the index with unequal variances. The multivariate linear regression equation with FR as the dependent variable and the residual deformity perimeters as the influential factors was established to analyze how the independent perimeters influence the FR.

Results

The data of each deformity perimeter were normally distributed. The FR was 79.72° (21.55°-120.11°) on average. For the radial deformities, the IRAR, RAR, and DAR were 82.69° (27.71°-176.76°), 13.20° (0.55°-33.93°), 21.69° (0.02°-43.24°) on average, respectively. For the ulnar deformities, the IRAU, UAU, and PAU were 56.33° (10.15°-159.04°), 5.46° (-7.68°-18.48°), and 10.20° (-13.82°-40.64°) on average, respectively. The RLOS was 0.21 (0.14–0.48) on average. The RAPAM was 0.40 (0.18–0.70) on average. Regarding the ulnar head dislocation and the RDUD at DRUJ, all of the ulnar heads showed a dorsal dislocation, and the RDUD was 0.53 (0.11–1.08) on average (Table 1).

Table 1
Average data of each perimeter

(N = 48)	Average	Maximum	Minimum
FR	79.72°	120.11°	21.55°
RAR	13.20°	33.93°	0.55°
DAR	21.69°	43.24°	0.02°
IRAR	82.69°	176.76°	27.71°
UAU	5.46°	18.48°	-7.68°
PAU	10.20°	40.64°	-13.82°
IRAU	56.33°	159.04°	10.15°
RLOS	0.21	0.48	0.14
RAPAM	0.40	0.70	0.180
RDUD	0.53	1.08	0.11

Pearson correlation analysis results show that the FR had a strong correlation with the DAR (0.601, $P < 0.01$), a moderate correlation with the IRAR (0.552, $P < 0.01$) and IRAU (0.421, $P < 0.01$), and a low correlation with the PAU (0.286, $P = 0.048$), whereas the FR had no correlation with the RAR, UAU, RLOS, RAPAM, and RDUD (Table 2).

Table 2
Pearson correlation analysis between FR and other perimeters

Pearson coefficient	FR	
(N = 48)	r	P
DAR	0.601	< 0.001
IRAR	0.552	< 0.001
IRAU	0.421	0.003
PAU	0.286	0.048
RLOS	0.259	0.076
UAU	0.230	0.116
RAR	0.040	0.789
RAPAM	-0.276	0.058
RDUD	0.238	0.103

The IRAR had a low correlation with the DAR (0.347, P = 0.016). The UAU had a moderate correlation with the PAU (9.543, P < 0.01), whereas the PAU had a low correlation with the IRAU (0.378, P < 0.01).

Table 3
Multiple linear regression analysis of the forearm deformity equation

	Unstandardized Coefficients		**t**	**Sig.**
	β	**SE**		
constant	35.896	7.065	5.081	0.000
DAR	0.989	0.240	4.125	0.000
IRAR	0.271	0.078	3.454	0.001
F = 22.064, R = 0.704, adjusted R2 = 0.473 (P < 0.01)				

A scatterplot between each deformity and the FR was mapped (Fig. 8). It can be seen that there was no linear relationship between the RAPAM and the FR. The homogeneity of variance between each perimeter and the FR was tested, and the RDUD was eliminated. Taking the FR as the dependent variable and the other residual deformities perimeters as the influencing factors, the multiple linear regression equation was established (Table 3). The results showed that the forearm deformity equation was as follows: FR = 35.896 + 0.989 DAR + 0.271 IRAR.

Discussion

CRUS is a rare congenital deformity in clinical practice and the most common kind of CRUS is type 3 of the Cleary and Omer classification. Children may experience difficulty in participating activities like perineum sanitation and using utensils, thus develop a variety of psychological problems as they grow up as well. Even the adult patients may experience a low self-esteem. Therefore, surgical treatment is recommended.[6]

In recent years, the Kanaya technique has been used to reconstruct the anatomical structure of PRUJ and restore the forearm rotation function. This procedure has resolved the problem of re-ankylosis.[5–10] However, the outcome is expected to be improved further.

Previous studies[11–13] have shown that the deformity of the CRUS forearm is complex, which consists of several independent deformities, including radial deformities, ulnar deformities, deformities at the proximal part of radius and ulna, and the deformities at the distal part of radius and ulna, among others. These independent deformities, such as radial and ulnar deformities, are associated with the severity of fixed forearm rotation deformity. However, there is no relevant research investigating on which of these independent deformities is the most important factor affecting the fixed forearm rotation deformity.

In this study, we explored the weighting perimeter of the major influential factors related to the severity of forearm rotation deformity, laying a foundation for further improvement of the treatment of CRUS.

The digital reconstruction technology was used to reconstruct the osseous structure of the forearms of 48 patients with type 3 deformities, and the results showed that all the patients had radial and ulnar deformities, osseous synostosis at PRUJ, and deformities at the proximal and distal part of the radius and ulna, which were consistent with the results of previous research.[1, 2, 11–13]

To investigate the relationship of the deformity perimeters and the FR, the Pearson correlation test among the deformity perimeters was performed, which showed that the FR had a strong correlation with the DAR (0.601, $P < 0.01$), moderate correlation with the IRAR (0.552, $P < 0.01$) and IRAU (0.421, $P < 0.01$), and low correlation with the PAU (0.286, $P = 0.048$). The DAR had a low correlation with the IRAR (0.347, $P = 0.016$) and IRAU (0.369, $P = 0{,}01$). The results suggested that for the FR, the most influential deformity was the DAR, the IRAR and IRAU also had much influence on the FR and they were not correlated with each other, the other deformities seemed had little influence on the FR.

Then, to qualify this relationship, the multiple linear regression analysis of each deformity perimeter was performed, which established the relationship equation between the forearm deformity severity and other independent deformity perimeters (forearm deformity equation): $FR = 35.896 + 0.989\ DAR + 0.271\ IRAR$. The results suggest that the DAR and IRAR may greatly contribute to the severity of forearm rotation deformity, compared to other independent deformities.

The IRAU had a moderate correlation with the FR, but was excluded in the forearm deformity equation; thus, the IRAU had a little correlation with the FR, which was not entirely consistent with previous research.[13] Thus, the moderate Pearson correlation between these two deformities may be a result of confounding factors.

In this study, the average RAPAM was 0.4, which was less than half of the normal area. Moreover, given that the shape and development of the radial heads are far from the normal in type 3 cases, which are often in the shape of a sharp cone, it is difficult to have a radial head in a correct shape after surgery. This may affect the postoperative alignment of the humeroradial joint, thereby affecting the outcomes of forearm rotation and elbow stability. This may be one of the reasons that caused the poor postoperative forearm rotation function and complications.

This study still has several limitations. First, given that the disease is a rare congenital malformation, the sample size of this study was small, the results may be biased. Second, all the cases in this study were classified as type 3, which makes this study has little importance to the other types of CRUS. Third, the age of the patients ranged from 1 to 28 years old, and the data were not grouped and analyzed by age, which may bias the results.

In a summery, among the deformities caused by the CRUS, the DAR and IRAR may be the most important indicators affecting the severity of forearm rotation deformities, whereas the IRAU and PAU did not highly correlate with FR. The forearm deformity equation was as follows: FR = 35.896 + 0.989 DAR + 0.271 IRAR. The results of this study might play some role in designing the treatment strategy in the future.

Declarations

Ethics approval: The experimental protocol was established, according to the ethical guidelines of the Helsinki Declaration and was approved by the Human Ethics Committee of

Beijing Ji Shui Tan hospital (202003-02). Written informed consent was obtained from individual or guardian participants.

Consent for publication: Not applicable.

Availability of data and material: The datasets used or analyzed during the current study are available from the corresponding author on reasonable request.

Declaration of interest: The authors declare that they have no competing interests

Funding: Supported by Beijing Natural Science Foundation (7192082, L192052).

Authors' contributions: Chen Yang, Lu Liu is responsible for the article writing and data analysis, Shan-lin Chen is responsible for check and approve, Qi-pei Wei and Fan Bai is responsible for the data collection.

Acknowledgment: I would like to thank Ms. Shen for her help during the article revision process. Their efforts are very important.

References

1. Green WT, Mital MA. Congenital radio-ulnar synostosis: surgical treatment. J Bone Joint Surg Am. 1979;61(5):738–43.
2. Cleary JE, Omer GE Jr. Congenital proximal radio-ulnar synostosis. Natural history and functional assessment. J Bone Joint Surg Am. 1985;67(4):539–45.
3. Ramachandran M, Lau K, Jones DH. Rotational osteotomies for congenital radioulnar synostosis. J Bone Joint Surg Br. 2005;87(10):1406–10. DOI:10.1302/0301-620X.87B10.16445.
4. Rubin G, Rozen N, Bor N. Gradual correction of congenital radioulnar synostosis by an osteotomy and Ilizarov external fixation. J Hand Surg Am. 2013;38(3):447–52. DOI:10.1016/j.jhsa.2012.10.037.
5. Kanaya F. Mobilization of congenital proximal radio-ulnar synostosis: a technical detail. Tech Hand Up Extrem Surg. 1997;1(3):183–8. DOI:10.1097/00130911-199709000-00005.
6. Shan-lin Chen Lu, Liu. De-di Tong. Treatment of Congenital Proximal Radioulnar Synostosis Using Pedicle Posterior Interosseous Perforator Adipofasical Flaps. Chin J Plast Surg. 2019;35(9):881–6. DOI:10.3760/cma.j.issn.1009-4598.2019.09.007.

7. Funakoshi T, et al. The use of pedicled posterior interosseous fat graft for mobilization of congenital radioulnar synostosis: a case report. J Shoulder Elbow Surg. 2004;13(2):230–4. DOI:10.1016/j.jse.2003.09.009.
8. Bell SN, Benger D. Management of radioulnar synostosis with mobilization, anconeus interposition, and a forearm rotation assist splint. J Shoulder Elbow Surg. 1999;8(6):621–4. DOI:10.1016/s1058-2746(99)90101-5.
9. Kawaguchi S, Kitamura M, Usui M. Proximal radioulnar synostosis treated with a free vascularised fascio-fat graft–report of two cases. Hand Surg. 2000;5(2):161–4. DOI:10.1142/s0218810400000302.
10. Sotereanos DG, Sarris I, Chou KH. Radioulnar synostosis after the two-incision biceps repair: a standardized treatment protocol. J Shoulder Elbow Surg. 2004;13(4):448–53. DOI:10.1016/j.jse.2004.01.030.
11. Dawson HG, A CONGENITAL DEFORMITY OF. THE FOREARM AND ITS OPERATIVE TREATMENT. Br Med J. 1912;2(2701):833–5.
12. Greig DM. Observations on the Bones in Congenital Proximal Radio-Ulnar Synostosis. Edinb Med J. 1925;32(7):354–69.
13. Nakasone M, et al. Three-dimensional analysis of deformities of the radius and ulna in congenital proximal radioulnar synostosis. J Hand Surg Eur Vol. 2018;43(7):739–43. DOI:10.1177/1753193417753261.

Figures

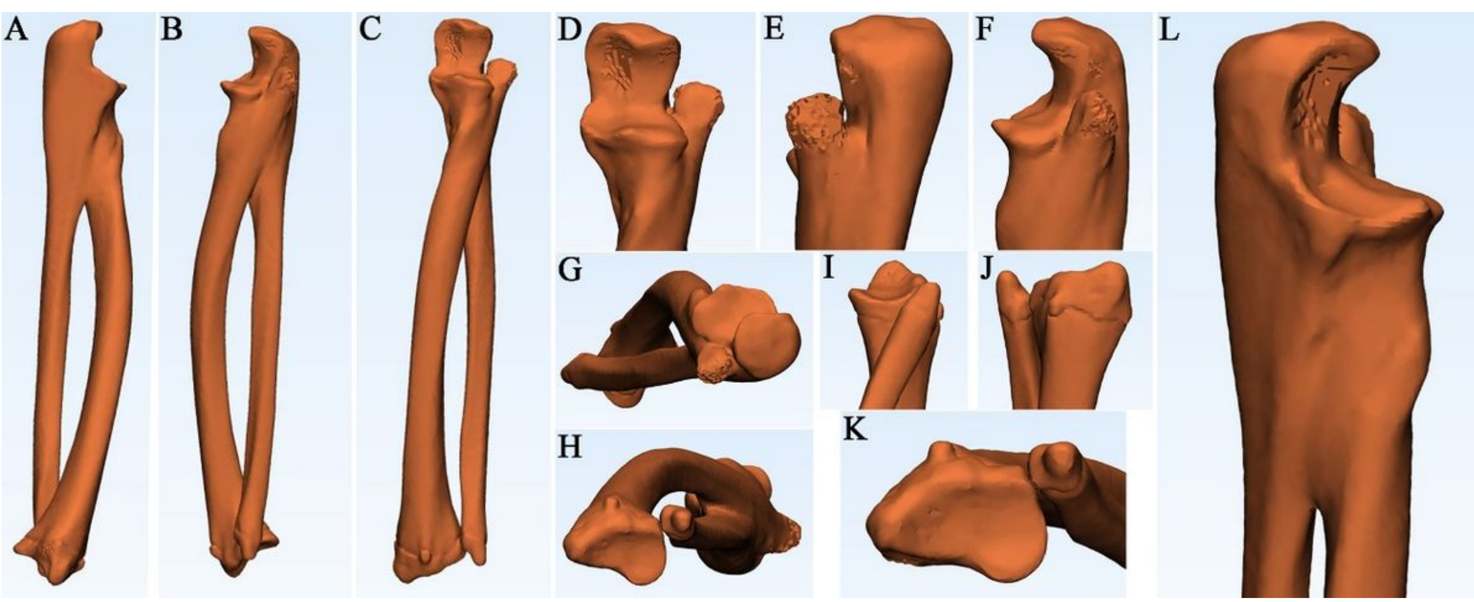

Figure 1

Abnormal osseous structures of CPRUS. A, B, C: radial and ulnar lateral angulation deformity; D, E, F: deformity at proximal part of radius and ulna; G, H: internal rotation deformity of radius and ulna; I, J, K:

deformity at distal part of radius and ulna; L: osseous synostosis of the PRUJ.

Figure 2

Measurement method of the forearm rotation angle. angle A represented the forearm rotation angle (FR).

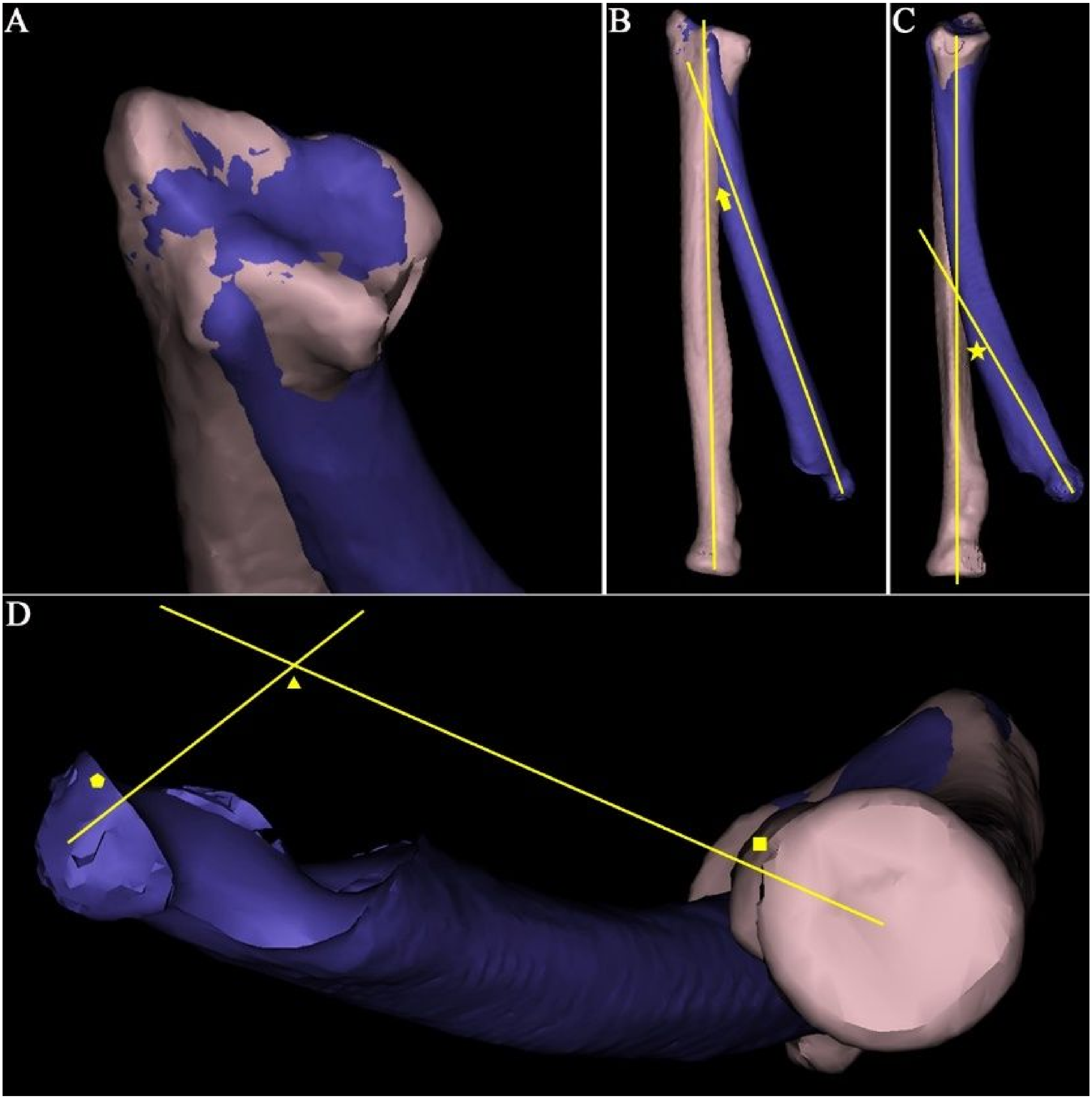

Figure 3

Measurement methods of radial deformities. A: distal radial articular surfaces were superimposed; B, C, D: the arrow, star and triangle represented the RAR, DAR, IRAR, respectively. D: the rectangle and pentagon represented the projection of the cutting edge at the proximal part of the affected radius and the incisura ulnaris, respectively.

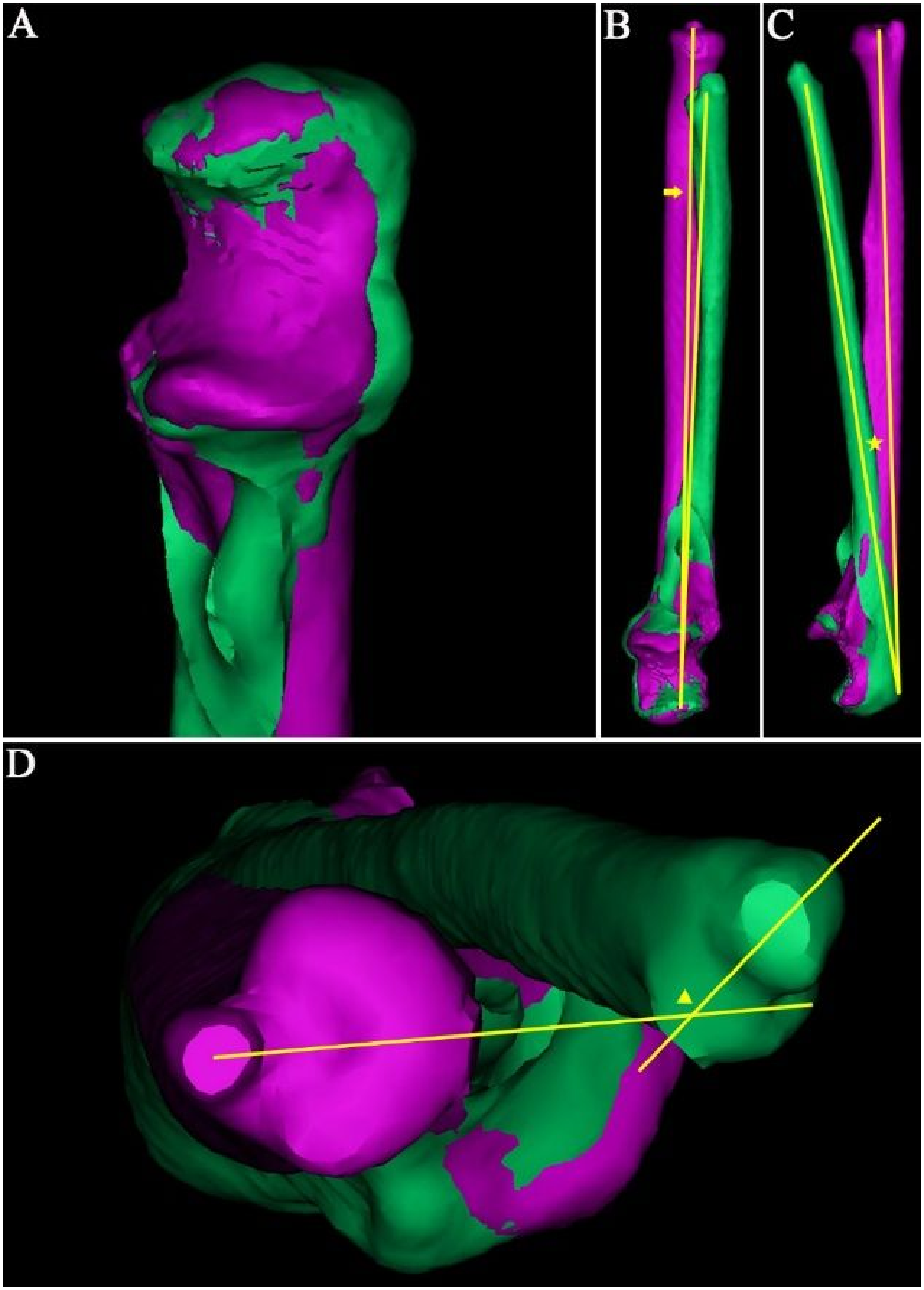

Figure 4

Measurement methods of ulna deformities. A: humeroulnar articular surfaces and olecranon were superimposed; B, C, D: the arrow, star and triangle represented the UAU, PAU and IRAU, respectively.

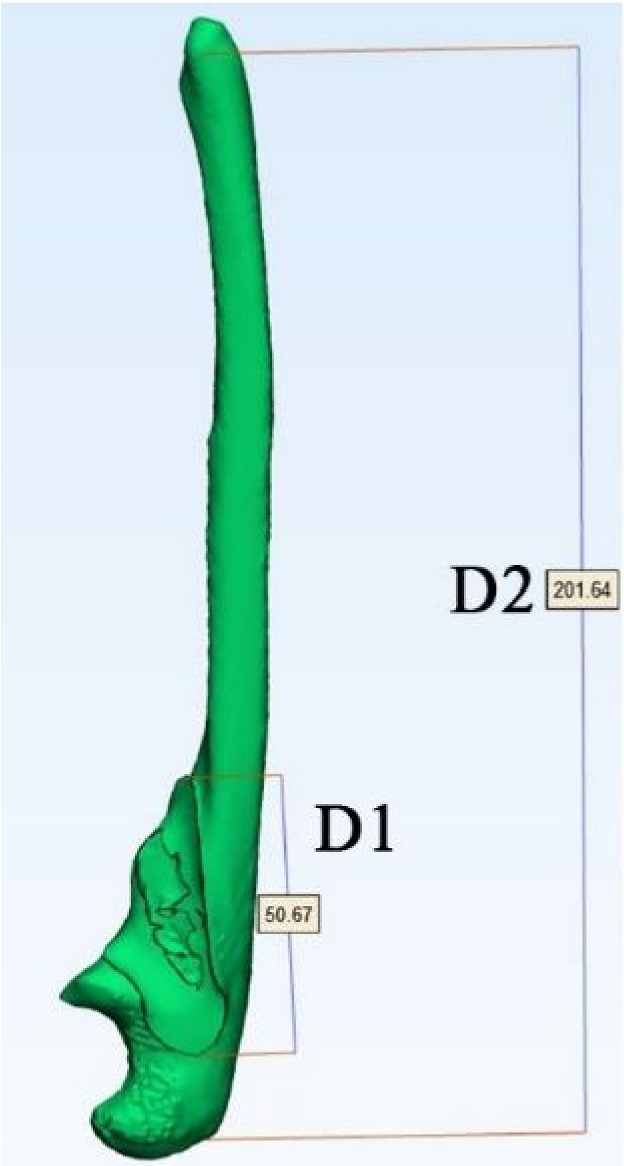

Figure 5

Measurement method of the RLOS (D1/D2). D1: the longest diameter of the fusion site(removed) of the affected ulna; D2: the distance between the center of the ulna head and the midpoint of the olecranon tip.

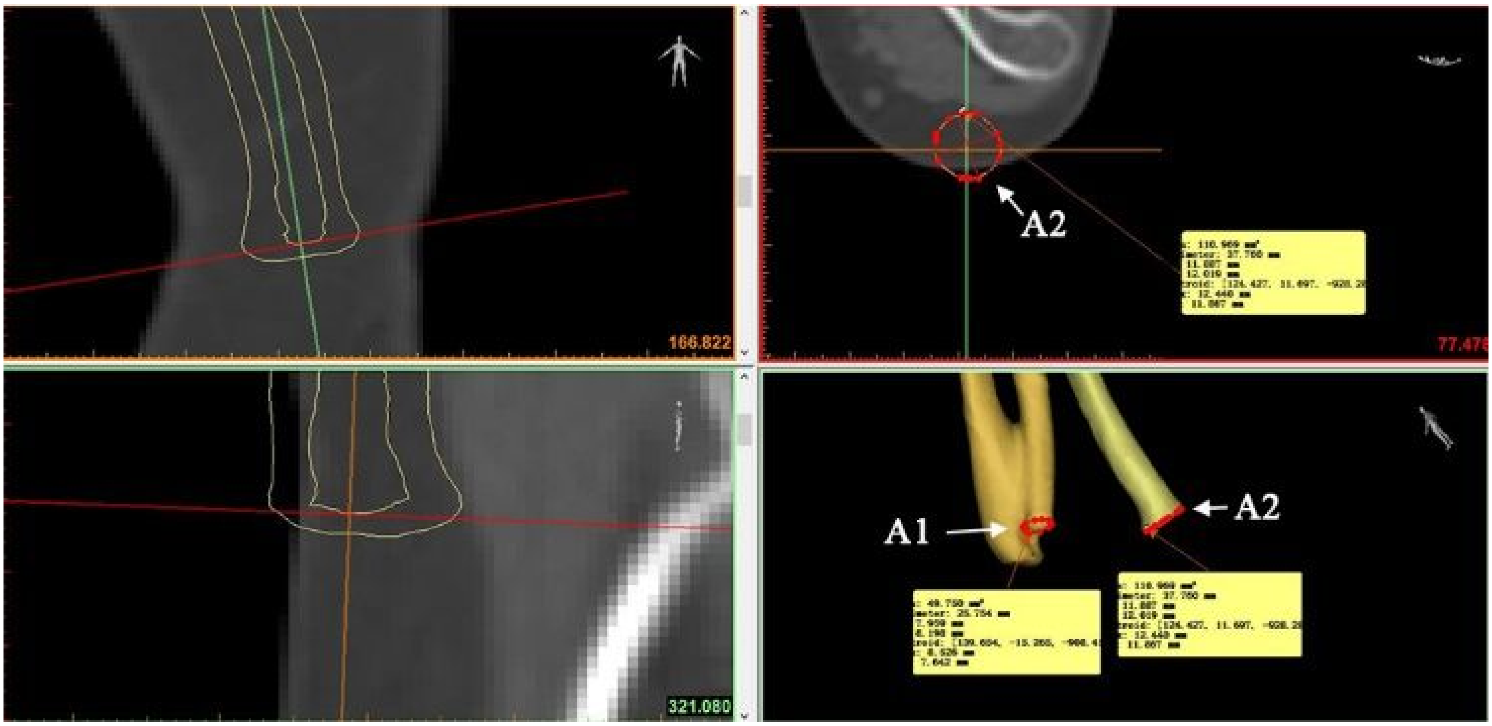

Figure 6

Measurement method of the RAPAM (A1/A2). A1: the transverse area of the proximal metaphysis of the affected radius; A2: the transverse area of the proximal metaphysis of the healthy radius.

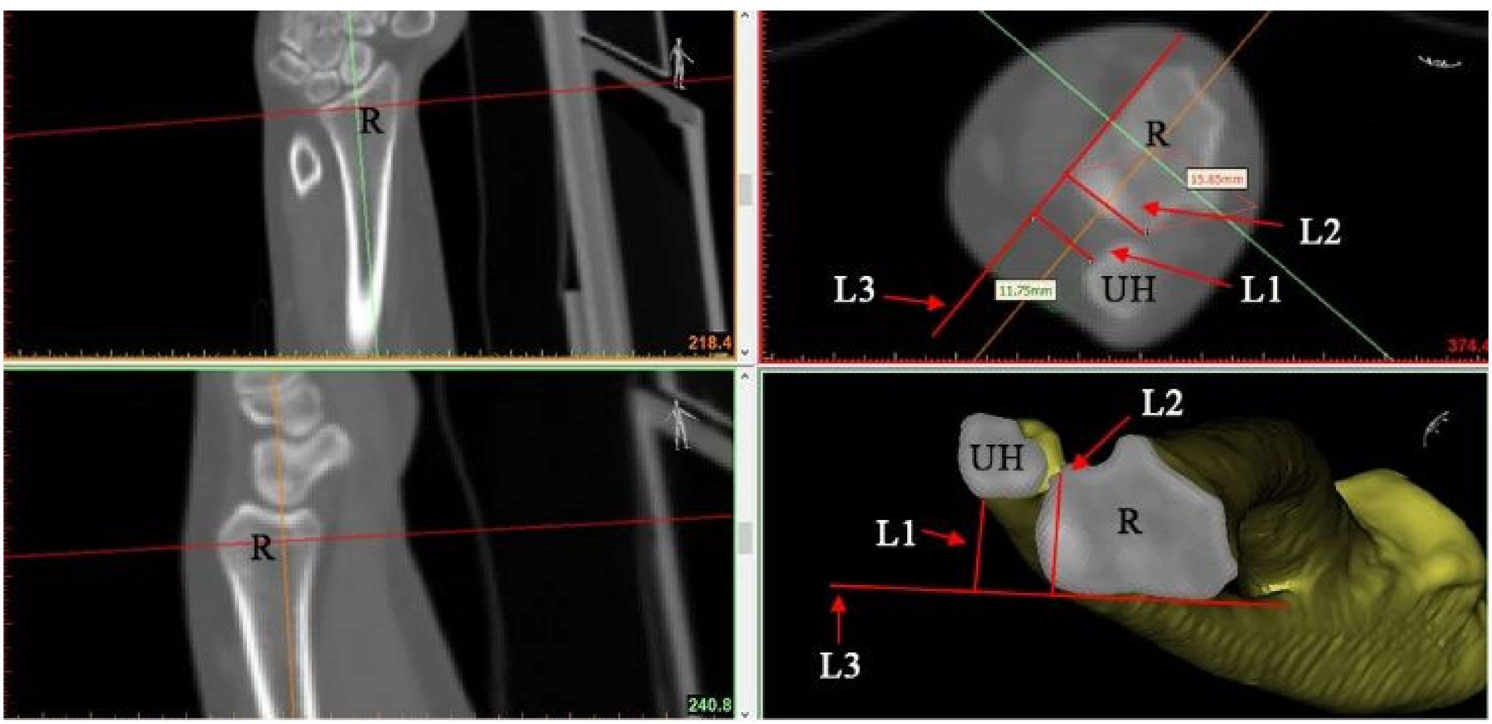

Figure 7

Measurement method of the RDUD(L1/L2). L1: the vertical distance between the palmar margin of the ulnar head and the extension line of the radial palmar margin; L2: the length of the sigmoid notch; L3: the extension line of the radial palmar margin; UH: ulnar head; R: radius.

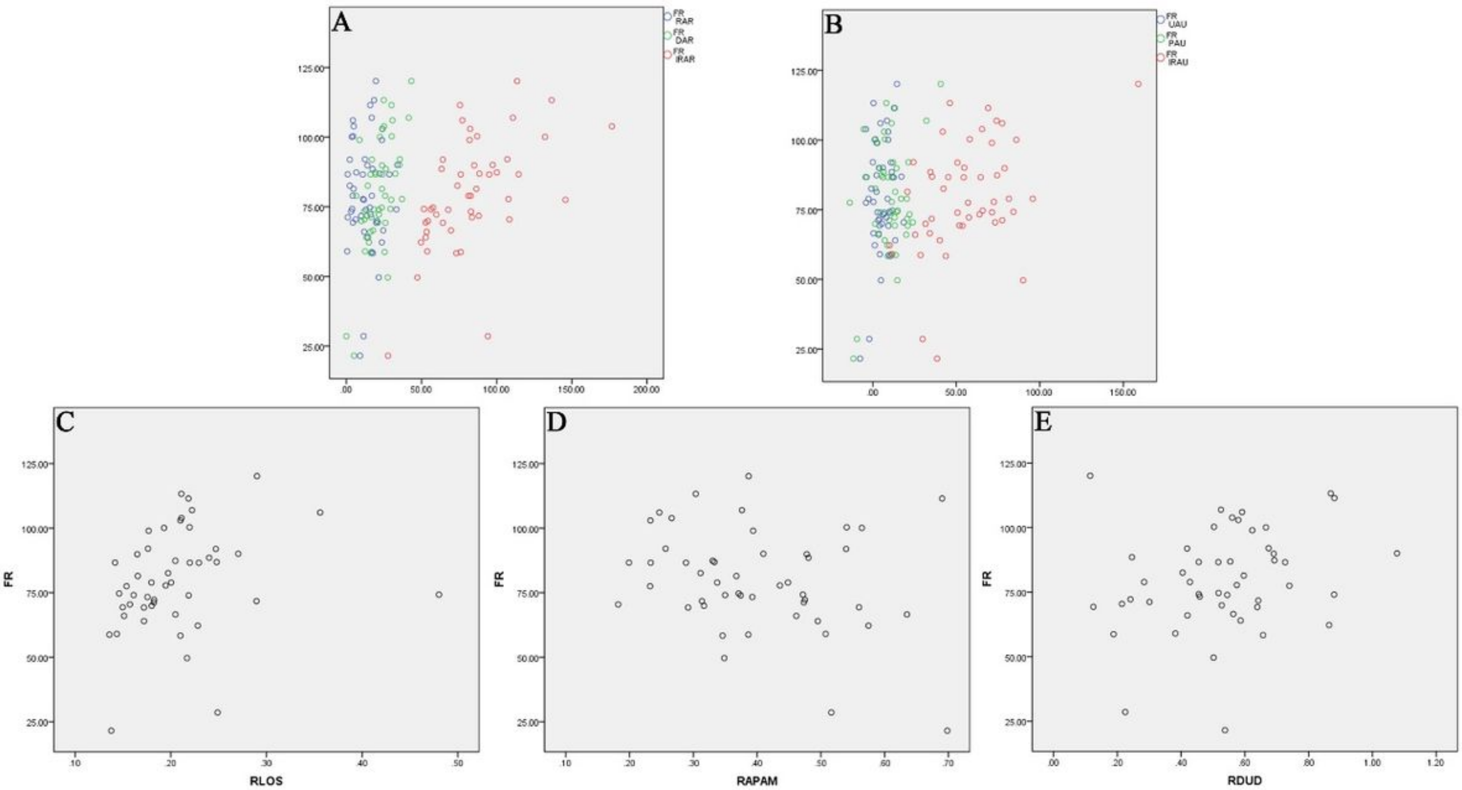

Figure 8

Scatterplot between each deformity perimeter and the FR. Y axis in each scatterplot was the FR. A: the blue dots, the green dots, the red dots represented the UAU, PAU, IRAU, respectively. B: the blue dots, the green dots, the red dots represented the RAR, DAR, IRAR, respectively. C, D, E: X axis in each scatterplot was the RLOS, RAPAM, RDUD, respectively.

Supplementary Files

This is a list of supplementary files associated with this preprint. Click to download.

- Supplementary1.docx